Joint migration velocity analysis of PP- and PS-waves for VTI media

Pengfei Cai[1] and Ilya Tsvankin[2]

ABSTRACT

Combining PP-waves with mode-converted PS reflections in migration velocity analysis (MVA) can help build more accurate VTI (transversely isotropic with a vertical symmetry axis) velocity models. To avoid problems caused by the moveout asymmetry of PS-waves and take advantage of efficient MVA algorithms designed for pure modes, here we generate pure SS-reflections from PP and PS data using the PP + PS = SS method. Then the residual moveout in both PP and SS common-image gathers is minimized during iterative velocity updates. The model is divided into square cells, and the VTI parameters V_{P0}, V_{S0}, ε, and δ are defined at each grid point. The objective function also includes the differences between the migrated depths of the same reflectors on the PP and SS sections. Synthetic examples confirm that 2D MVA of PP- and PS-waves may be able to resolve all four relevant parameters of VTI media if reflectors with at least two distinct dips are available. The algorithm is also successfully applied to a 2D line from 3D ocean-bottom seismic data acquired at Volve field in the North Sea. After the anisotropic velocity model has been estimated, accurate depth images can be obtained by migrating the recorded PP and PS data.

INTRODUCTION

Prestack depth migration (PSDM) and reflection tomography in the migrated domain are widely used in P-wave imaging (Stork, 1992; Wang et al., 1995; Adler et al., 2008; Bakulin et al., 2010). Most current PSDM and migration velocity analysis (MVA) algorithms account for transverse isotropy with a vertical (VTI) or tilted (TTI) symmetry axis. Sarkar and Tsvankin (2004) develop an efficient MVA method for P-waves in VTI media by dividing the model into factorized blocks. Within each block, the anisotropy parameters

ε and δ are constant, while the P-wave symmetry-direction velocity V_{P0} varies linearly in space. To extend P-wave MVA to more complex subsurface structures, Wang and Tsvankin (2013) suggest a ray-based tomographic algorithm in which the parameters V_{P0}, ε, and δ are defined on a rectangular grid, while the symmetry axis is fixed perpendicular to reflectors. Similar multiparameter tomographic inversion for TTI media is applied to synthetic and field P-wave data by Zhou et al. (2011).

To resolve the velocity V_{P0} and anisotropy parameters ε and δ required for P-wave depth imaging, it is necessary to combine P-wave traveltimes with additional information. Tsvankin and Thomsen (1995) demonstrate that long-spread (nonhyperbolic) P- and SV-wave moveouts in horizontally layered VTI media are sufficient for estimating the parameters V_{P0}, ε, δ, and the shear-wave vertical velocity V_{S0}. It is more practical, however, to supplement P-waves with converted PS(PSV) data. For 2D VTI models, the parameters V_{P0}, V_{S0}, ε, and δ can be obtained by combining PP- and PS-wave traveltimes for a horizontal and dipping interface (Tsvankin and Grechka, 2000). For a stack of horizontal VTI layers, however, the combination of PP and PS moveouts does not constrain the interval Thomsen parameters (Grechka and Tsvankin, 2002a).

Several authors discuss joint tomographic inversion of PP and PS data (Audebert et al., 1999; Stopin and Ehinger, 2001; Broto et al., 2003; Foss et al., 2005). However, velocity analysis of mode conversions is hampered by the asymmetry of PS moveout (i.e., PS traveltimes generally do not stay the same when the source and receiver are interchanged) and polarity reversals of PS-waves. As discussed by Thomsen (1999), Grechka and Tsvankin (2002b), and Tsvankin and Grechka (2011), the apex of the PS moveout in common-midpoint (CMP) gathers typically is shifted from zero offset. Therefore, MVA for PS-waves (Audebert et al., 1999; Foss et al., 2005; Du et al., 2012) has to account for the "diodic" nature of PS reflections (Thomsen, 1999). For example, common-image gathers (CIGs) of PS-waves can be computed separately for positive and negative offsets in the tomographic objective function (Foss et al., 2005).

To replace mode conversions in velocity analysis with pure SS reflections, Grechka and Tsvankin (2002b) suggest the so-called PP + PS = SS method. By combining PP and PS events that share P-legs, that method generates SS reflection data with the correct kinematics for arbitrarily anisotropic, heterogeneously media. Grechka et al. (2002b) perform joint inversion of PP and PS reflection data for TI models using stacking-velocity tomography (Grechka et al., 2002a), which operates with NMO velocities for 2D lines and NMO ellipses for wide-azimuth 3D surveys. They first construct SS traveltimes with the PP + PS = SS method and then apply stacking-velocity tomography to the acquired PP and computed SS data. However, their methodology is limited to hyperbolic moveout and excludes information contained in long-offset traveltimes. Also, stacking-velocity tomography can handle only relatively simple layered or blocked models.

To make use of efficient MVA techniques for pure modes (Sarkar and Tsvankin, 2004; Wang and Tsvankin, 2013), here we apply the kinematic version of the PP + PS = SS method to construct pure SS-wave reflections from PP and PS data. Then MVA is performed by simultaneously flattening PP- and SS-wave CIGs. Our parameter-updating procedure is based on the gridded reflection tomography developed for P-waves by Wang and Tsvankin (2013). PP- and SS-wave images of the same reflector do not match in depth if the velocity model is incorrect (e.g., Tsvankin and Grechka, 2011). Therefore, in addition to removing residual moveout in image gathers, we penalize depth misties between the migrated PP and SS sections.

First, we introduce our velocity-analysis methodology, which includes identification (registration) of PP and PS events from the same interfaces, application of the PP + PS = SS method to create SS reflection data, and joint reflection tomography of the recorded PP- and generated SS-waves. Next, the algorithm is tested on a horizontal VTI layer sandwiched between isotropic media and on a layered model that includes a dipping reflector (e.g., a fault plane). The results confirm that if reflections from two different dips are available, the joint MVA can resolve the VTI parameters of piecewise-homogeneous models without additional information. Finally, we
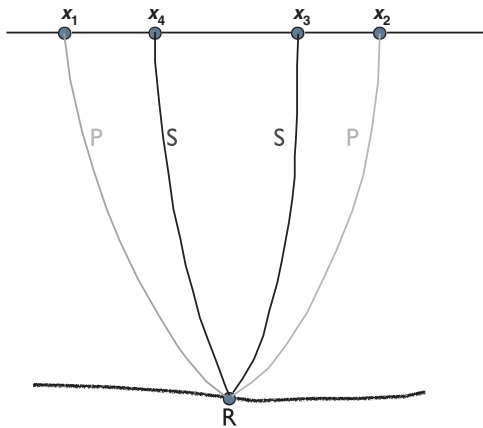
apply the algorithm to a more complex model with a laterally heterogeneous VTI syncline and to field data from the North Sea.

METHODOLOGY

P-wave reflection traveltimes generally are insufficient to resolve the parameters V_{P0}, ε, and δ required for P-wave depth imaging in VTI media. Therefore, to build a VTI model for prestack depth migration, at least one medium parameter (e.g., V_{P0}) must be known a priori (e.g., Sarkar and Tsvankin, 2004).

As discussed in Tsvankin and Grechka (2000), combining P-wave traveltimes with the moveout of PS-waves converted at a horizontal and dipping interface can help constrain the vertical P- and S-wave velocities and the parameters ε and δ. The most significant problem in PS-wave velocity analysis is the moveout asymmetry with respect to zero offset in CMP geometry (Tsvankin and Grechka, 2011). Unless the model is laterally homogeneous and has a horizontal symmetry plane, the PS traveltime does not stay the same when the source and receiver are interchanged. Therefore, most MVA methods designed for pure modes cannot be directly applied to converted waves. Here, we employ the PP + PS = SS method (Grechka and Tsvankin, 2002b) to produce pure SS primary reflection events using PP and PS reflections from the same interface.

Implementation of the PP + PS = SS method requires prior event registration, or identification of PP and PS reflections from the same boundaries. The main idea of the method is to combine PP and PS events that share the same P-legs. This is done by matching time slopes (horizontal slownesses) on common-receiver gathers of PP- and PS-waves (Figure 1). Then the traveltime of the constructed SS wave (sometimes called the "pseudo-S" arrival; its trajectory is $x_3 R x_4$) is given by

$$t_{SS}(x_3, x_4) = t_{PS}(x_1, x_3) + t_{PS}(x_2, x_4) - t_{PP}(x_1, x_2). \quad (1)$$

Note that whereas the constructed SS-wave traveltimes are exact, the PP + PS = SS method cannot produce correct reflection amplitudes.

Grechka and Dewangan (2003) develop a convolution-based procedure designed to compute SS-wave seismograms from recorded PP and PS traces. The main advantage of this "full-waveform" version of the PP + PS = SS method is that it does not require traveltime picking. However, convolution involves integration of traces over all sources and receivers and is computationally expensive. Hence, here we apply the kinematic version of the PP + PS = SS method and convolve the computed SS traveltimes with a Ricker wavelet to generate "pseudo" SS reflection data for MVA.

Because SS-waves are obtained from mode conversions, the offsets of the constructed SS reflections are much smaller than the corresponding PP-wave offsets (Figure 1). Furthermore, the maximum reflection angle of the shear wave generated by a P-to-S mode conversion in a horizontal isotropic layer with the P- and S-wave velocities V_P and V_S is $\theta_S^{crit} = \sin^{-1}(V_S/V_P)$. Therefore, the half-offset h_S of the computed SS-wave cannot exceed the critical value (Figure 2),

$$h_S^{crit} = D \tan\left[\sin^{-1}\left(\frac{V_S}{V_P}\right)\right], \quad (2)$$

Figure 1. Matching the horizontal slownesses on common-receiver PP and PS gathers at locations x_1 and x_2 helps find the source-receiver coordinates x_3 and x_4 of the pure SS ray $x_3 R x_4$. This reconstructed SS ray has the same reflection point R as the PP ray $x_1 R x_2$ and PS rays $x_1 R x_3$ and $x_2 R x_4$ (after Grechka and Tsvankin, 2002b).

where D is the layer's thickness. For example, for a typical $V_S/V_P = 1/2$, the maximum half-offset is less than $0.6D$. Therefore, it is necessary to include long-offset PP and PS data with offset-to-depth ratios reaching two. This physical constraint makes it necessary to include long-offset PP and PS data (with offset-to-depth ratios reaching two) to generate SS-waves suitable for robust velocity analysis (Grechka and Tsvankin, 2002b).

Here, we extend the P-wave MVA algorithm of Wang and Tsvankin (2013) to multicomponent (PP and SS) data. The model is divided into square cells, and the parameters V_{P0}, V_{S0}, ε, and δ are defined at each grid point. We apply Kirchhoff prestack depth migration to both recorded PP and constructed SS data, starting with initially isotropic velocity models in the synthetic examples below. In practice, the initial model may be obtained from stacking-velocity tomography at borehole locations (Wang and Tsvankin, 2010) or nonhyperbolic moveout analysis (as done in the case study below). The moveouts of migrated PP and SS events in CIGs serve as input to the joint MVA.

To constrain the anellipticity parameter $\eta \equiv (\varepsilon - \delta)/(1 + 2\delta)$ (and, therefore, ε), the moveout in PP-wave CIGs is described by the nonhyperbolic equation (Sarkar and Tsvankin, 2004):

$$z^2(h) = z^2(0) + Ah^2 + B\frac{h^4}{h^2 + z^2(0)}, \quad (3)$$

where z is the migrated depth as a function of the half-offset h, and the coefficients A and B are found by a 2D semblance scan. There is no need to include the term proportional to h^4 in equation 3 for SS-wave CIGs because the offset-to-depth ratio of the constructed SS events seldom exceeds 1–1.2. In addition to minimizing the residual moveout in PP- and SS-wave CIGs, we also perform codepthing, which involves tying PP and SS images of the same reflectors. The objective function includes a term that penalizes the mismatch in depth of PP and SS migrated images using a selection of key reflection points chosen on the basis of coherency and reflector focusing (Foss et al., 2005).

The model update is obtained by minimizing the objective function introduced below. To solve the minimization problem, it is necessary to compute traveltime derivatives with respect to the model parameters (Wang and Tsvankin, 2013). Since we operate with PP- and SS-waves, the parameter set includes not just V_{P0}, ε, and δ, but also the shear-wave vertical velocity V_{S0}. The exact P- and SV-wave phase velocities in VTI media can be expressed as (Tsvankin, 2005)

$$\frac{V^2}{V_{P0}^2} = 1 + \varepsilon\sin^2\theta - \frac{f}{2}$$
$$\pm \frac{f}{2}\sqrt{1 + \frac{4\sin^2\theta}{f}(2\delta\cos^2\theta - \varepsilon\cos 2\theta) + \frac{4\varepsilon^2\sin^4\theta}{f^2}}, \quad (4)$$

where θ is the phase angle with the symmetry axis and $f \equiv 1 - V_{S0}^2/V_{P0}^2$. The plus sign in front of the radical corresponds to the velocity of P-waves and minus to the velocity of SV-waves. For purposes of MVA, however, it is convenient to replace ε and δ with the P-wave horizontal ($V_{hor,P}$) and NMO ($V_{nmo,P}$) velocities

given by $V_{hor,P} = V_{P0}\sqrt{1 + 2\varepsilon}$ and $V_{nmo,P} = V_{P0}\sqrt{1 + 2\delta}$, so that all unknowns have the units of velocity. We compute the traveltime derivatives with respect to $V_{hor,P}$ and $V_{nmo,P}$ instead of ε and δ. The MVA algorithm updates V_{P0}, V_{S0}, $V_{hor,P}$, and $V_{nmo,P}$ and then converts $V_{hor,P}$ and $V_{nmo,P}$ into ε and δ.

The objective function used in the joint MVA of PP- and SS-waves is defined as follows:

$$F(\Delta\lambda) = \mu_1\|\mathbf{A}_P\,\Delta\lambda + \mathbf{b}_P\|^2 + \mu_2\|\mathbf{A}_S\,\Delta\lambda + \mathbf{b}_S\|^2$$
$$+ \mu_3\|\mathbf{D}\,\Delta\lambda + \mathbf{y}\|^2 + \zeta\|L\Delta\lambda\|^2, \quad (5)$$

where $\Delta\lambda$ is the update of the vector λ of medium parameters, the matrices $\mathbf{A}_P$ and $\mathbf{A}_S$ include the derivatives of the PP and SS migrated depths with respect to the elements of λ (medium parameters), the vectors $\mathbf{b}_P$ and $\mathbf{b}_S$ contain elements that characterize the residual moveout in PP- and SS-wave CIGs, the matrix $\mathbf{D}$ describes the differences between the derivatives of the PP and SS migrated depths with respect to the medium parameters, and the vector $\mathbf{y}$ contains the differences between the migrated depths on the PP and SS sections. The full definitions of $\mathbf{A}_P$, $\mathbf{A}_S$, $\mathbf{D}$, $\mathbf{b}_P$, $\mathbf{b}_S$, and $\mathbf{y}$ are given in Appendix A. Minimizing the first two terms ($\|\mathbf{A}_P\,\Delta\lambda + \mathbf{b}_P\|^2$ and $\|\mathbf{A}_S\,\Delta\lambda + \mathbf{b}_S\|^2$) allows us to flatten PP and SS CIGs, and codepthing is achieved through minimizing the third term ($\|\mathbf{D}\,\Delta\lambda + \mathbf{y}\|^2$). Because the tomographic inversion can be ill-posed, we add a regularization term ($\|L\Delta\lambda\|$) to the objective function. The coefficients μ_1, μ_2, μ_3, and ζ govern the weights of the corresponding terms.

The objective function is minimized by a least-squares algorithm. Since the VTI parameters are updated at each grid point, which makes the inversion time-consuming, we parallelize our code. CIGs for each reflector are computed on different cores, and flattening of PP and SS events is performed simultaneously.

TESTS ON SYNTHETIC DATA

Models composed of homogeneous layers

We use anisotropic ray-tracing package ANRAY to generate PP- and PS-wave reflection traveltimes for synthetic tests (Gajewski and Pšenčík, 1987). PP and SS images are generated with Kirchhoff prestack depth migration using Seismic Unix (SU) program "sukdmig2d." To create traveltime tables of PP- and SS-waves, we perform ray tracing for heterogeneous VTI media using SU code "rayt2dan."

We first test the algorithm on a simple horizontally layered model (Figure 3) that includes a VTI layer sandwiched between isotropic media. In the absence of dips, the interval parameters for this model
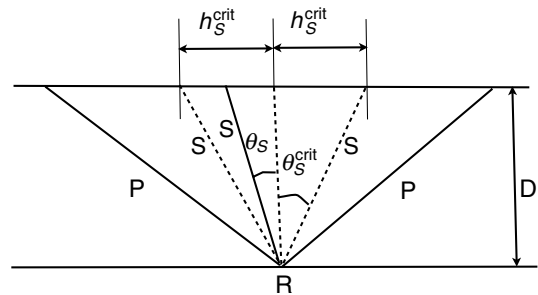

Figure 2. Critical (maximum) offset $2h_S^{crit}$ of the constructed SS-waves in a horizontal layer (Tsvankin and Grechka, 2011).

cannot be constrained by PP and PS reflection traveltimes (Grechka and Tsvankin, 2002a; Tsvankin and Grechka, 2011). Therefore, the P-wave vertical velocity V_{P0} is assumed to be known, and we invert only for V_{S0} and the anisotropy parameters ε and δ of the VTI layer.

The top layer is known to be isotropic and its P- and S-wave velocities can be easily found from reflection data. The initial

S-wave vertical velocity in the middle VTI layer is 10% smaller than the true value, and both ε and δ are set to zero. The maximum offset-to-depth ratio for the bottom of the VTI layer is close to two, which is sufficient for applying the PP + PS = SS method. Indeed, the maximum offset for the constructed SS data is 1.6 km, and the corresponding offset-to-depth ratio exceeds unity. The entire PP data set is used along with the SS-waves to estimate the residual moveout in CIGs. For codepthing, however, we only use conventional-spread PP data with offsets not exceeding those for the constructed SS-waves.

The PP and SS image gathers computed with the initial model are not flat (Figure 4a and 4b), and the bottom of the VTI layer is not only poorly focused but also imaged at different depths on the PP and SS sections. CIGs used for velocity analysis are uniformly sampled from 1 to 3 km along the second reflector. Since we use gridded tomography, the derivatives of migrated depths with respect to the model parameters are calculated at the vertices of relatively fine grids. Therefore, we follow Wang and Tsvankin (2013) in employing a mapping matrix to convert the model updates into the parameter values at each grid point. After 10 iterations, the CIGs are flat (Figure 5a and 5b) and the reflectors are tied in depth
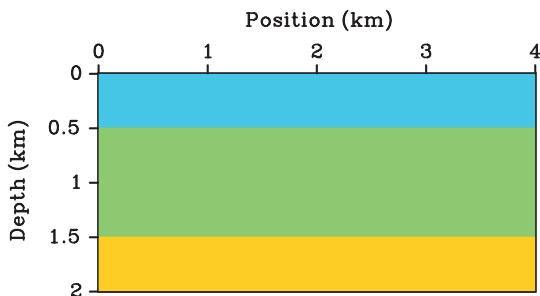

Figure 3. Model with a VTI layer embedded between two isotropic layers. The P- and S-wave velocities in the top layer are $V_P = 2000$ m/s and $V_S = 1000$ m/s; for the second layer, $V_{P0} = 3000$ m/s, $V_{S0} = 1500$ m/s, $\varepsilon = 0.1$, and $\delta = -0.1$.

Figure 4. CIGs of (a) PP-waves and (b) SS-waves (displayed every 100 m) for the model in Figure 3 after migration with the initial parameters.
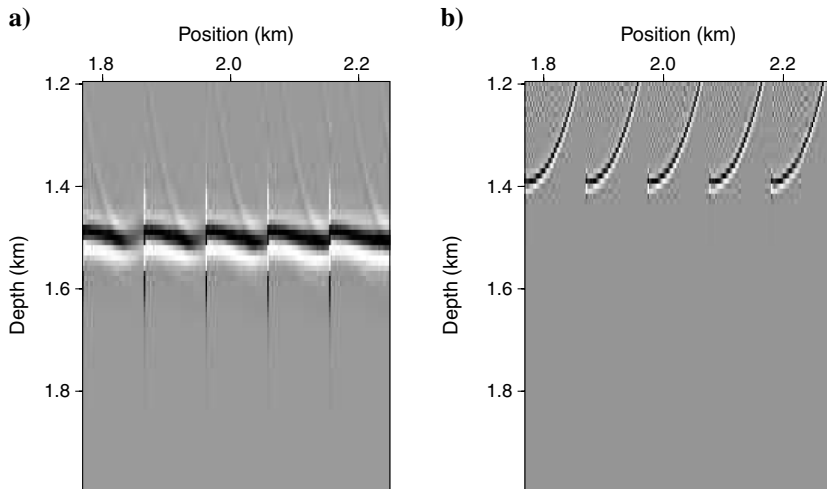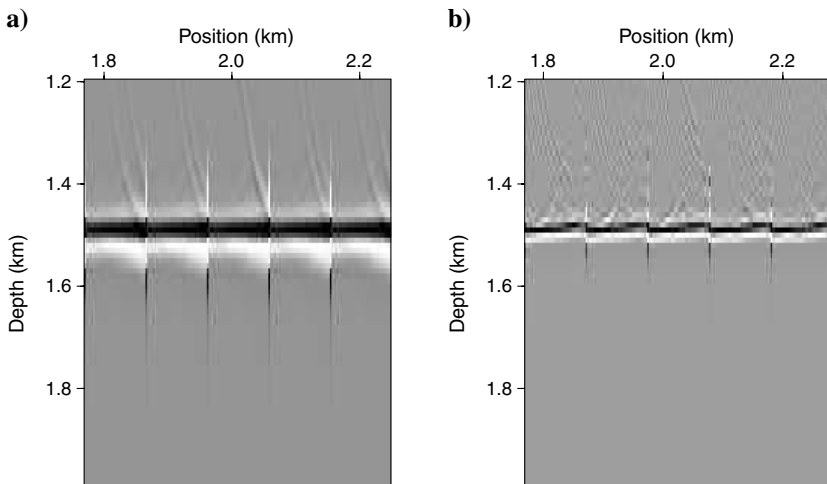

Figure 5. CIGs of (a) PP-waves and (b) SS-waves for the model in Figure 3 after migration with the inverted parameters.

(Figure 6a and 6b). The estimated parameters of the VTI layer are close to the actual values: $V_{S0} = 1494$ m/s, $\varepsilon = 0.1$, and $\delta = -0.09$ (V_{P0} is known).

Next, the algorithm is tested on a model (Figure 7) that includes a reflector (e.g., a fault plane) dipping at an angle of 27°. To avoid instability in ray tracing, the corner of the dipping interface is smoothed using bicubic spline interpolation. The synthetic data include PP and PS reflections from both horizontal and dipping reflectors (Figure 8). The maximum offsets are 4 km for the PP data and 2 km for the SS-waves constructed by the PP + PS = SS method. Tsvankin and Grechka (2000) demonstrate that the traveltimes of the PP- and PS-waves reflected from a horizontal and a dipping interface (with dips exceeding 15°) are sufficient to constrain the parameters V_{P0}, V_{S0}, ε, and δ.

Assuming the velocities in the subsurface layer to be known, we invert for the parameters of the middle VTI layer. The initial model is isotropic with the velocities V_{P0} and V_{S0} distorted by 15%. The initial V_{P0}/V_{S0} ratio, which can be accurately estimated from the zero-offset traveltimes, is correct. The depth sections computed with the initial model are displayed in Figure 9 (note the particularly poor quality of the SS section). A set of CIGs of PP- and SS-waves from both the horizontal and dipping interfaces (at locations from 1 to 4 km) are used in the joint MVA. After 11 iterations, the algorithm practically removes residual moveout in CIGs and the reflectors on the PP and SS sections are correctly positioned (Figure 10a and 10b). The inversion also produces accurate estimates of the interval VTI parameters: $V_{P0} = 3031$ m/s, $V_{S0} = 1515$ m/s, $\varepsilon = 0.20$, and $\delta = 0.08$. These results confirm the feasibility of building layered VTI depth models using 2D PP and PS reflection data if both horizontal and dipping events are available.
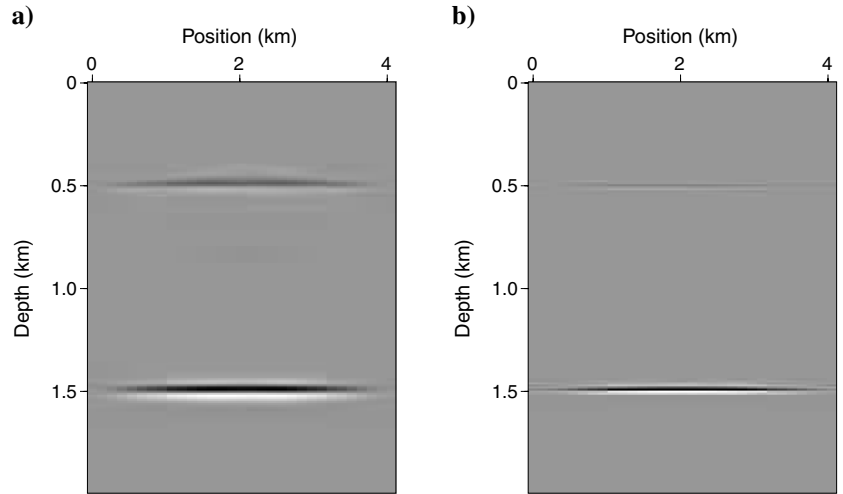

Figure 6. Final depth images of (a) PP-waves and (b) SS-waves obtained with the inverted parameters for the model in Figure 3.
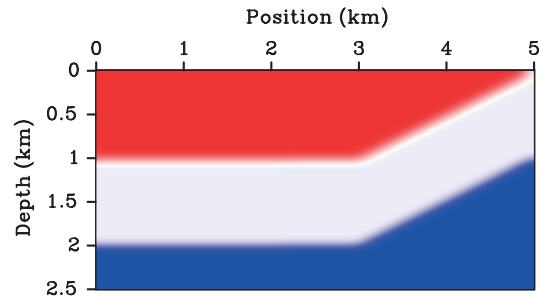

Figure 7. Three-layer model with dipping interfaces. The parameters of the top isotropic layer are $V_P = 2000$ m/s and $V_S = 1000$ m/s; for the second VTI layer, $V_{P0} = 3000$ m/s, $V_{S0} = 1500$ m/s, $\varepsilon = 0.2$, and $\delta = 0.1$. The maximum dip of both reflectors is 27°.
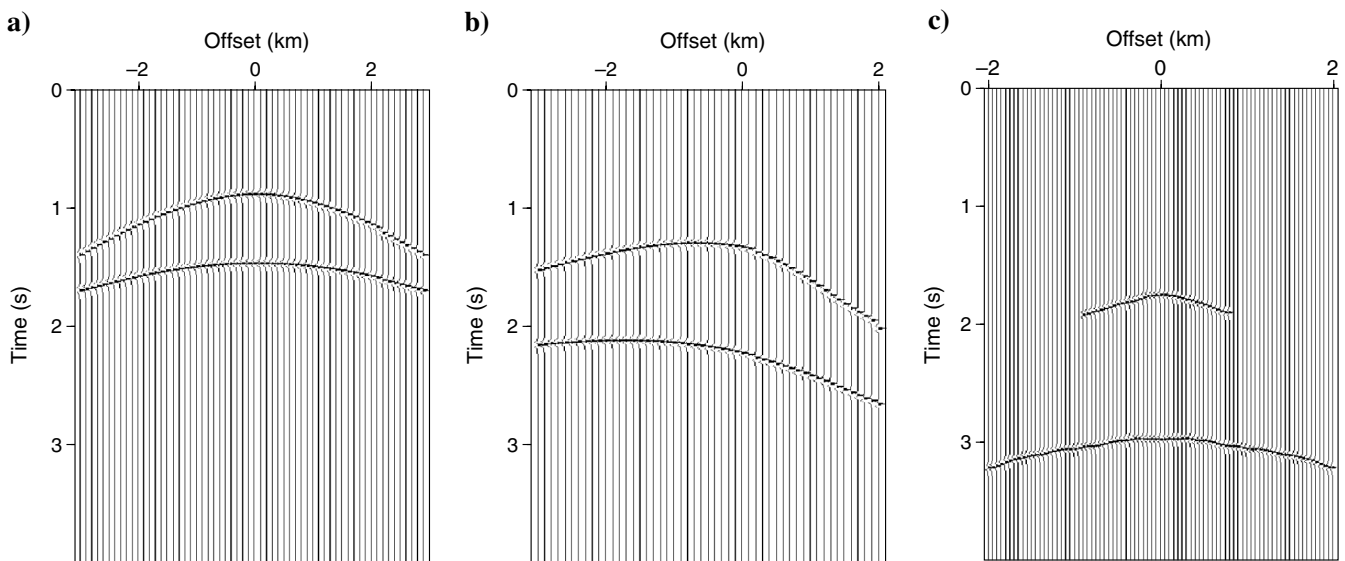

Figure 8. CMP gathers of the recorded (a) PP-waves and (b) PS-waves at location 3000 m for the model in Figure 7. (c) The SS data constructed by the PP + PS = SS method at the same location.

Model with heterogeneous layers

It is important to assess the ability of the algorithm to reconstruct spatial velocity variations along with the anisotropy parameters. Following Sarkar and Tsvankin (2004), we build a model with a factorized VTI layer, in which the ratios of the stiffness coefficients (and, therefore, the anisotropy parameters and the V_{P0}/V_{S0} ratio) are constant (Figure 11). The vertical velocities in the VTI layer vary linearly in space, with V_{P0} defined as

$$V_{P0}(x, z) = V_{P0}(x_0, z_0) + k_{p,x}(x - x_0) + k_{p,z}(z - z_0), \quad (6)$$

where (x_0, z_0) is an arbitrary point inside the layer, and $k_{p,x}$ and $k_{p,z}$ are the lateral and vertical gradients, respectively. Because the VTI layer is factorized, the velocity V_{S0} at each point is obtained by setting $V_{P0}(x, z)/V_{S0}(x, z) = 2$. The dip of the flanks of the syncline is about 27°, and the VTI layer contains an additional internal reflector. The P- and S-wave velocities in the top layer (known to be isotropic) can be obtained from PP and SS traveltimes. In the in-

version, we do not assume the VTI layer to be fully factorized (i.e., the ratio V_{P0}/V_{S0} is not fixed), but the anisotropy coefficients are kept constant. Also, in the first test, both V_{P0} and V_{S0} are taken to be linear functions of x and z, so V_{S0} is described by

$$V_{S0}(x, z) = V_{S0}(x_0, z_0) + k_{s,x}(x - x_0) + k_{s,z}(z - z_0). \quad (7)$$

The algorithm inverts for the parameters $V_{P0}(x_0, z_0)$, $V_{S0}(x_0, z_0)$, $k_{p,x}$, $k_{p,z}$, $k_{s,x}$, $k_{s,z}$, ε, and δ of the VTI layer.

The initial velocities V_{P0} and V_{S0} at the top of the middle layer (at the point marked by a black dot) are 10% smaller than the actual values, and $k_{p,x}$, $k_{p,z}$, $k_{s,x}$, $k_{s,z}$, ε, and δ of the initial model are set to zero. The PP- and SS-wave CIGs for the two reflectors in the VTI layer are not flat (Figure 12a and 12b), and these reflectors imaged with the initial model are poorly focused and shifted in depth (Figure 13a and 13b). Velocity analysis is performed for common-image gathers from 1 to 5 km, including both the left and right flanks of the syncline. The maximum offset-to-depth ratio for

Figure 9. (a) PP-wave and (b) SS-wave depth images for the model in Figure 7 computed with the initial parameters.
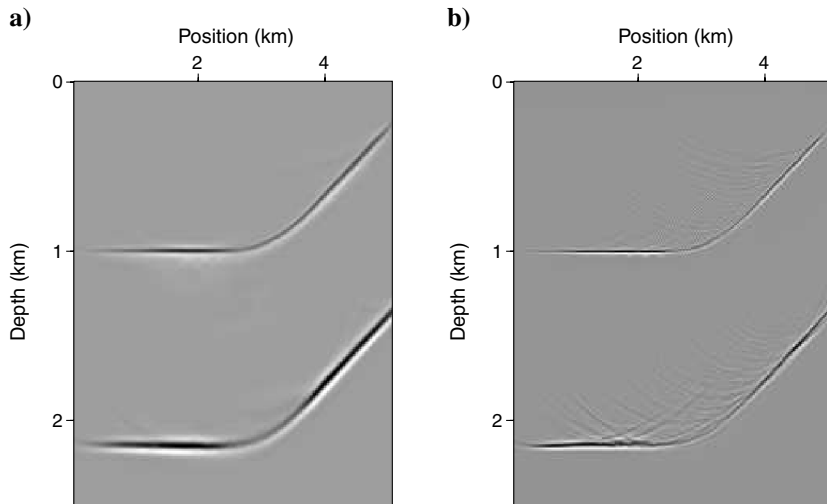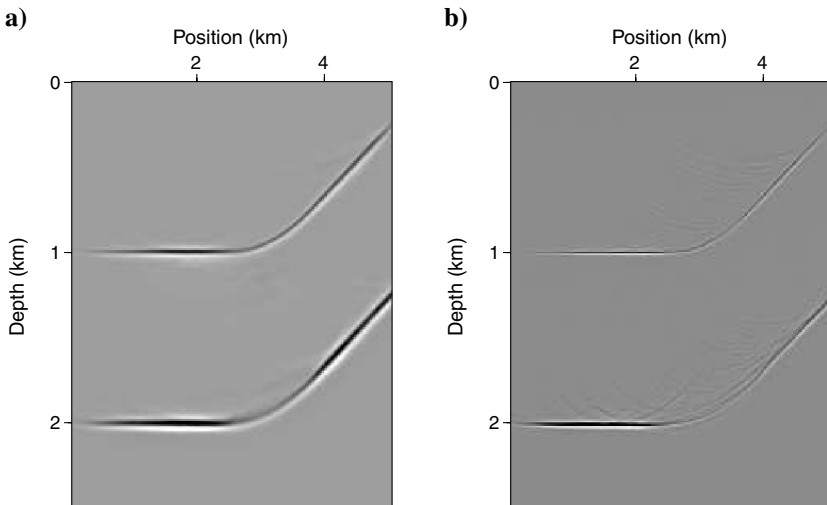

Figure 10. Final depth images of (a) PP-waves and (b) SS-waves for the model in Figure 7 obtained with the inverted parameters.
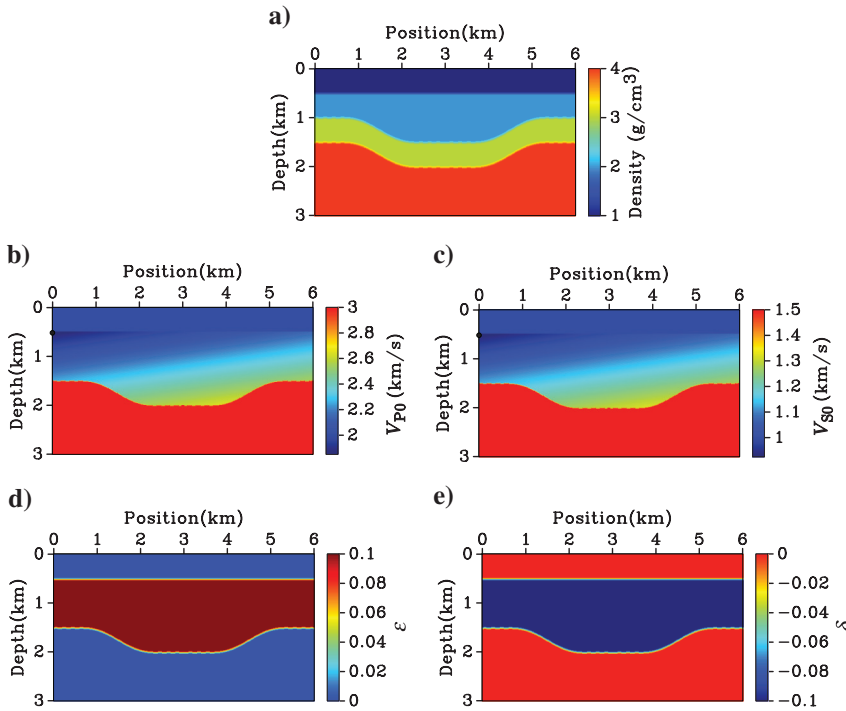
Figure 11. Model with a factorized VTI layer embedded between two isotropic homogeneous layers. (a) The density, the vertical velocities (b) V_{P0} and (c) V_{S0}, and the anisotropy parameters (d) ε and (e) δ. The parameters of the top layer are $V_P = 2000$ m/s and $V_S = 1000$ m/s. For the second layer, the vertical velocities at the point marked by the black dot on the left are $V_{P0} = 1850$ m/s and $V_{S0} = 925$ m/s. Both V_{P0} and V_{S0} vary linearly with the lateral gradients $k_{p,x} = 0.05$ s^{-1} and $k_{s,x} = 0.025$ s^{-1} and vertical gradients $k_{p,z} = 0.4$ s^{-1} and $k_{s,z} = 0.2$ s^{-1} so that $V_{P0}/V_{S0} = 2$. The anisotropy parameters of the VTI layer are constant: $\varepsilon = 0.1$ and $\delta = -0.1$.
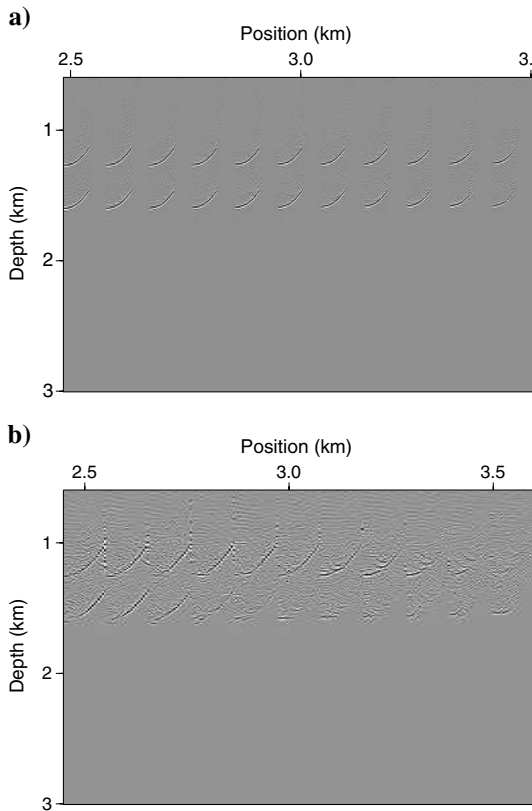

Figure 12. CIGs of (a) PP-waves and (b) SS-waves (displayed every 100 m) for the model in Figure 11 after migration with the initial parameters.
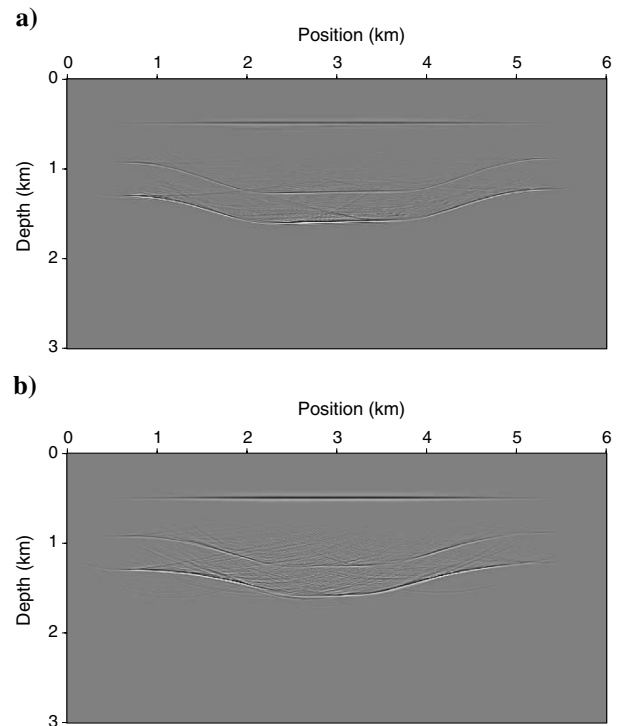

Figure 13. (a) PP-wave and (b) SS-wave depth images for the model in Figure 11 computed with the initial parameters.

the PP-wave CIGs is close to two, and it reduces to unity for the gathers of SS-waves.

After application of MVA to the two reflectors in the VTI layer, both PP and SS image gathers are flattened (Figure 14a and 14b), and PP and SS sections (Figure 15) are tied in depth. Making the correct (linear) assumption about V_{P0} and V_{S0} and keeping ε and δ constant helped resolve all four relevant VTI parameters (Table 1).

In the next test, the velocities V_{P0} and V_{S0} are updated at each grid point with no a priori constraints. However, the anisotropy parameters ε and δ in the VTI layer are still spatially invariant. The regularization term $\|\mathbf{L}\Delta\lambda\|$ applied in the inversion (equation 5) is a finite-difference approximation of the Laplacian operator.

The initial fields of V_{P0} and V_{S0} are obtained by reducing the actual values by 12% and 8%, respectively, and ε and δ are set

to zero. As a result, the reflectors in the VTI layer are shifted up and are somewhat deformed. Also, there is a mistie between the migrated PP and SS images at the bottom of the VTI layer. After nine iterations, joint tomography of PP- and PS-waves produces a good approximation for the parameter fields (Figure 16) and accomplishes the goal of flattening the image gathers and minimizing the depth misties (Figure 17). In particular, the mistie at the bottom of the VTI layer is reduced from 60 to 5 m. However, the quality of the final images in Figure 17 is not as high as that of the final sections in the previous test (Figure 15). We found that for laterally heterogeneous models the contribution of codepthing must be given a larger weight in the objective function during the last few iterations, whereas the first several updates can be mostly governed by the flattening-related terms.
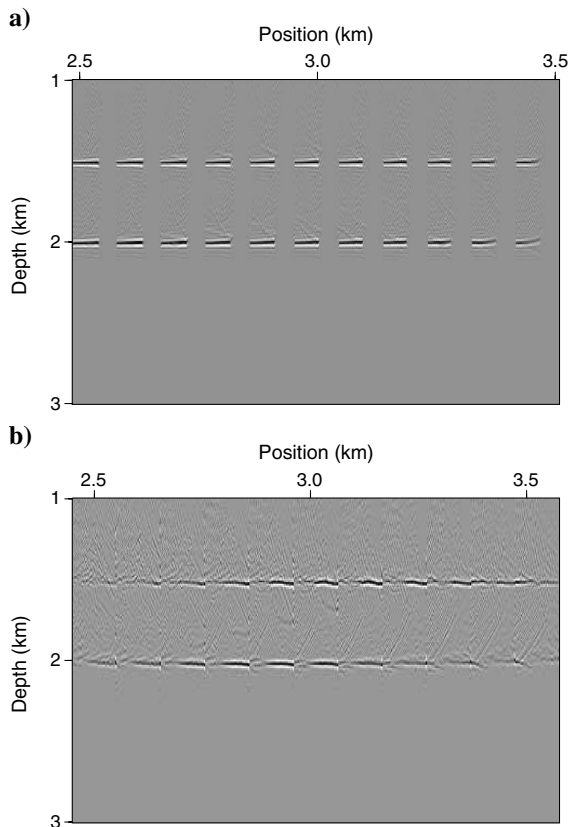

Figure 14. CIGs of (a) PP-waves and (b) SS-waves for the model in Figure 11 after migration with the inverted parameters (Table 1).
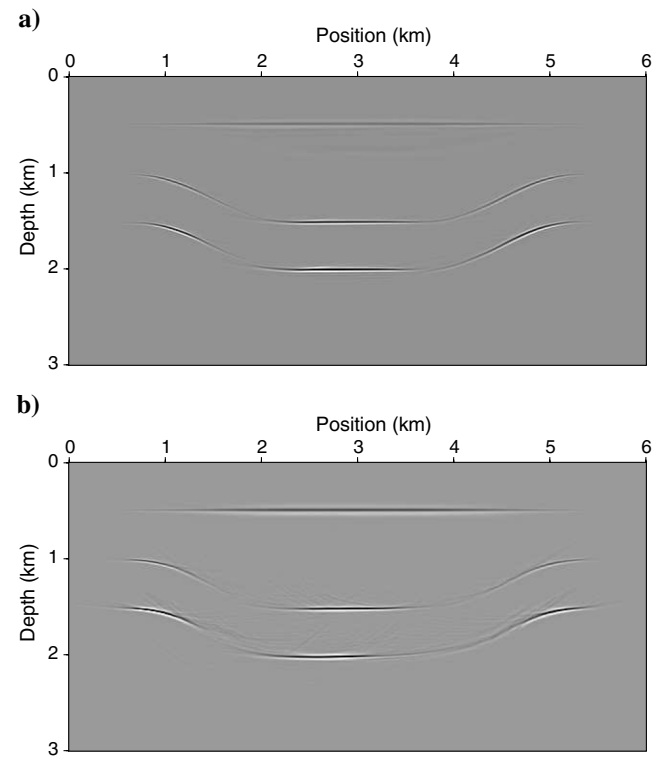

Figure 15. (a) PP-wave and (b) SS-wave depth images for the model in Figure 11 computed with the inverted parameters.

Table 1. Inversion results for the VTI layer from the model in Figure 11. The velocities V_{P0} and V_{S0} are correctly assumed to vary linearly inside the layer, and ε and δ are spatially invariant.

Model parameters	V_{P0} (m/s)	V_{S0} (m/s)	$k_{p,x}$(s^{-1})	$k_{p,z}$(s^{-1})	$k_{s,x}$(s^{-1})	$k_{s,z}$(s^{-1})	ε	δ
Actual	1850	925	0.05	0.4	0.025	0.2	0.1	−0.1
Initial	1665	833	0	0	0	0	0	0
Inverted	1873	945	0.043	0.42	0.023	0.21	0.11	−0.11
Error	1%	2%	−14%	5%	−8%	5%	0.01	−0.01

APPLICATION TO FIELD DATA

Next, the algorithm is applied to an offshore data set from Volve field provided to us by Statoil. Volve field is a Middle Jurassic oil reservoir located in the southern part of the Viking Graben in the gas/condensate-rich Sleipner area of the North Sea (Figure 18). The reservoir is in the Middle Jurassic Hugin Sandstone Formation and the deposition was controlled by salt tectonics (Szydlik et al., 2007).

An ocean-bottom seismic (OBS) survey was acquired in 2002 over a 12.3×6.8 km area of the field. It comprises six swaths of four-component (4C) data and each swath includes two 6 km-long cables placed on the seafloor. The cables have a 400 m spacing and move up 800 m after each swath. There are 240 receivers with an interval of
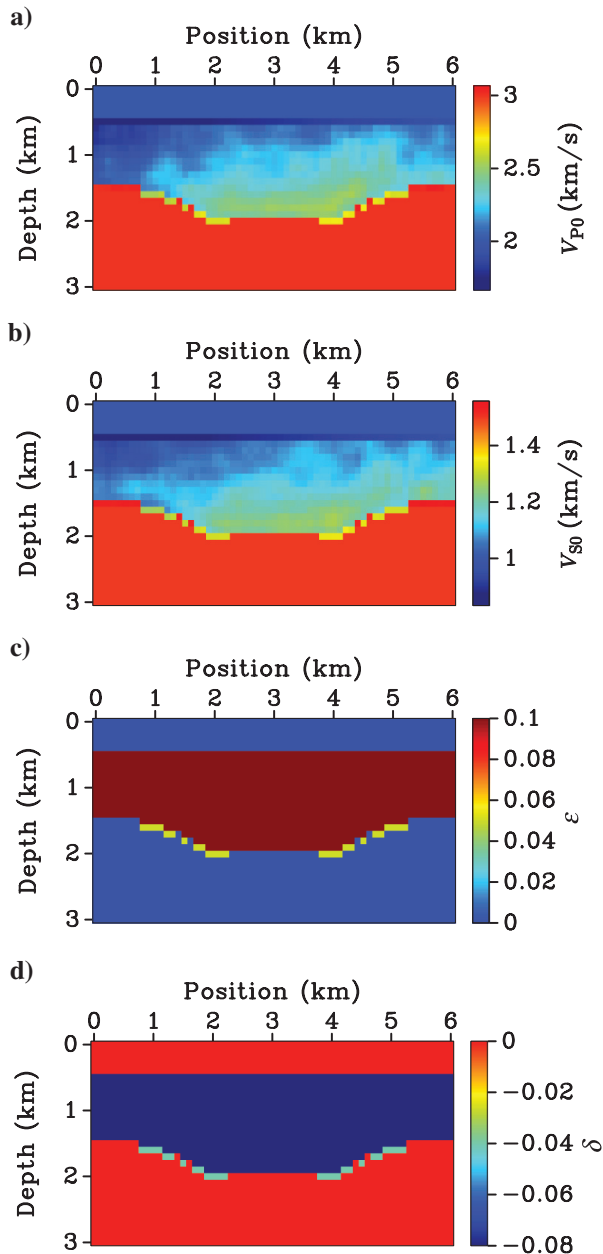
25 m on each cable. Dual-source flip-flop shooting gave a 25 m shot separation and a 100 m separation between sail lines.

The PP and PS OBS data were preprocessed using a standard sequence including wavelet shaping, noise and multiple attenuation techniques (Szydlik et al., 2007). The VTI model produced by Statoil for prestack depth imaging is built by applying layer-based tomography and fitting check-shot data (Szydlik et al., 2007). Complete information about the VTI model-building process employed by Statoil, however, is unavailable to us.

We use a 2D section from the 3D PP- and PS-wave data recorded by the cable laid along $y = 2.8$ km. PP-waves from the same line were processed by Wang (2012), who built a TTI model using reflection tomography. Two adjacent source lines ($y = 2.8 \pm 0.025$ km) include 481 shots with a shot interval of 25 m.

The joint MVA of PP- and PS-waves described above is applied to the CIGs from $x = 3$ km to 9 km with an interval of 100 m. The initial model for the parameters V_{P0}, ε, and δ is taken from Wang (2012), who divided the section into eight layers based on key geologic horizons and applied nonhyperbolic moveout analysis in combination with check shots. Since check-shot data for shear waves were not available, a smoothed version of the shear-wave vertical-velocity model provided by Statoil is used here as the initial V_{S0}-field. The parameters V_{P0}, V_{S0}, ε, and δ are defined on a 100×50 m grid (Figure 19).

The PP and PS images migrated with the initial model are shown in Figure 20. There is a clearly visible mistie between the PP and PS sections for a reflector at a depth close to 2.5 km (top of the Cretaceous Unit); the depth of that reflector is smaller on the PS image.

Figure 16. Velocities (a) V_{P0} and (b) V_{S0} for the model in Figure 11 estimated on a grid. Inverted layer-based parameters (c) ε and (d) δ.
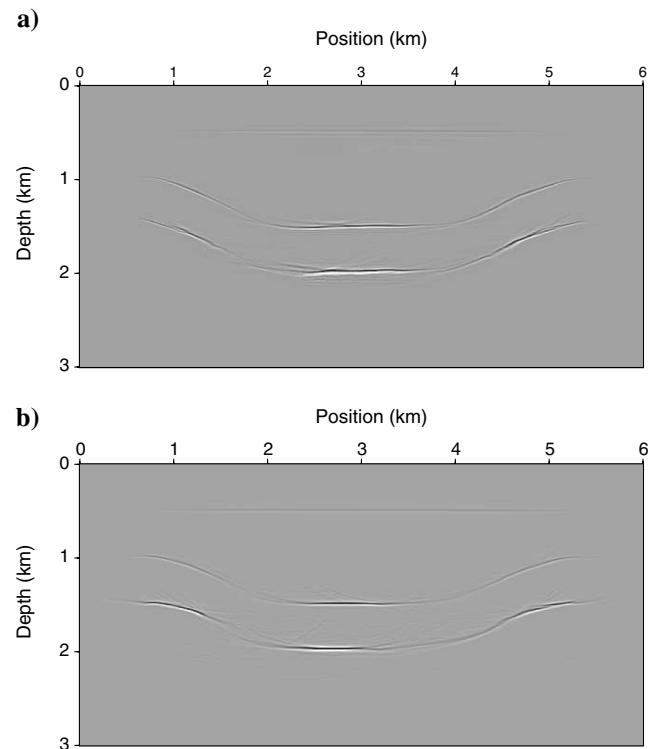

Figure 17. (a) PP-wave and (b) SS-wave depth images computed with the inverted parameters from Figure 16.

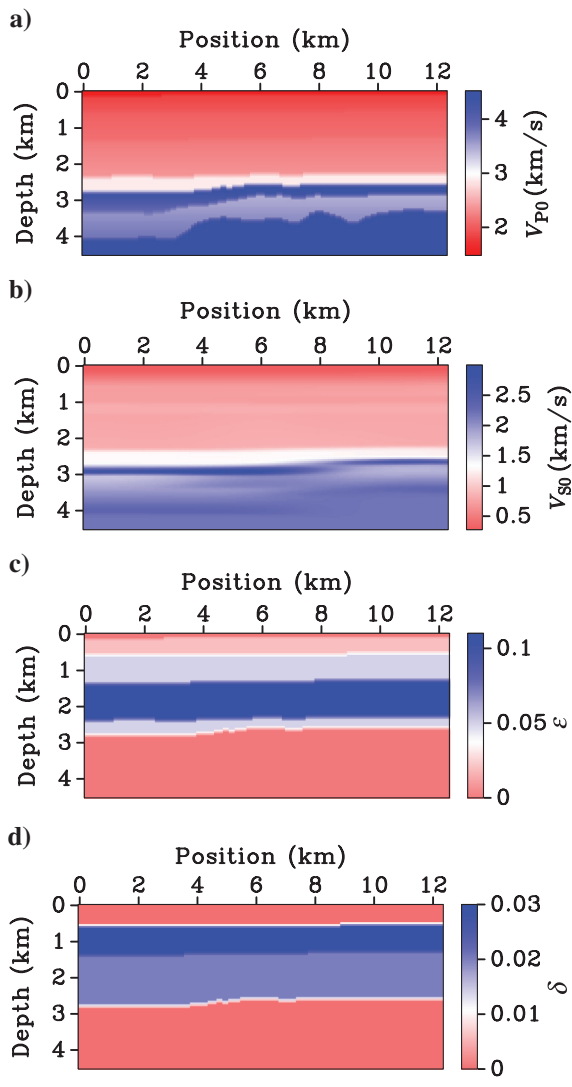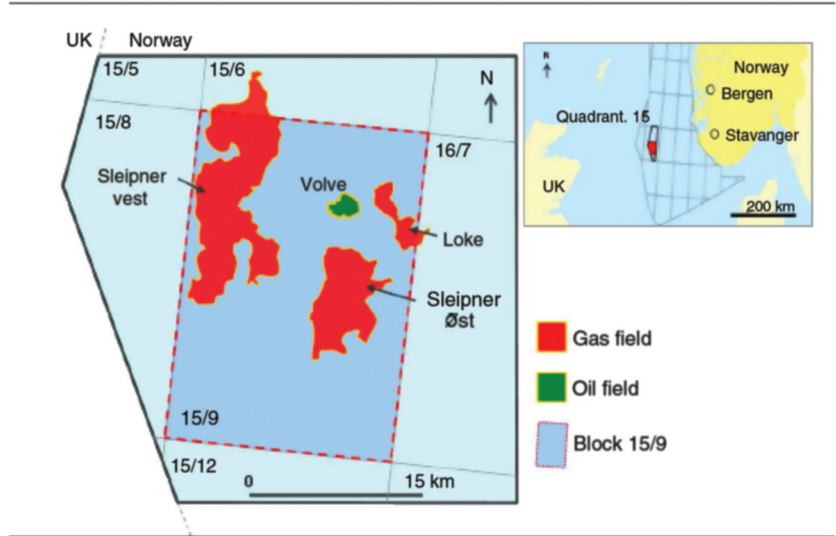Figure 18. Location of Volve field in the North Sea (figure courtesy of Statoil).

Figure 19. Initial VTI model for line $y = 2.8$ km from the Volve survey. The vertical velocities (a) V_{P0} and (b) V_{S0} and the anisotropy parameters (c) ε and (d) δ.
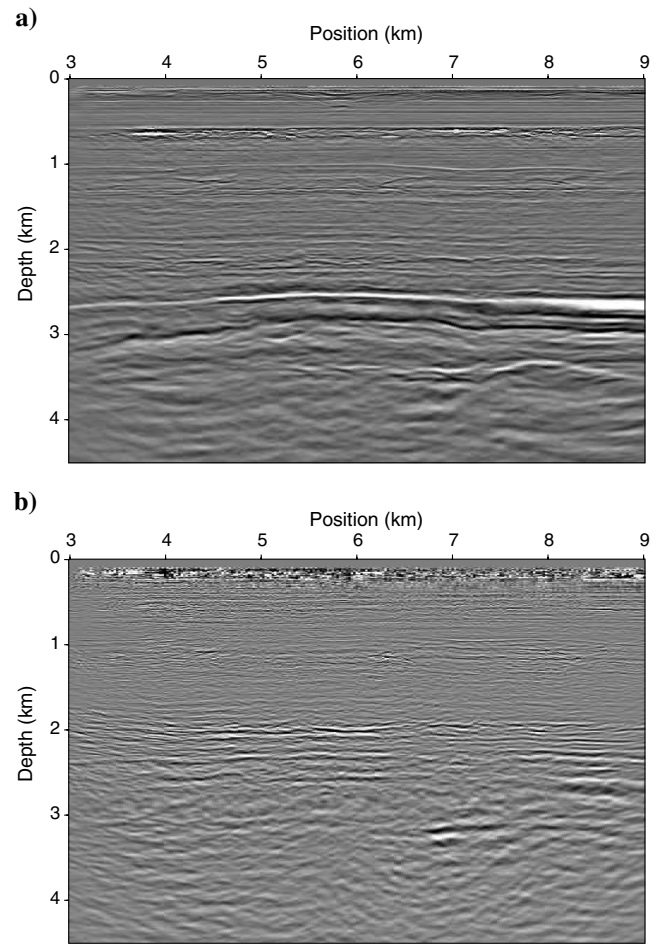
Figure 20. (a) PP- and (b) PS-wave images generated by Kirchhoff prestack depth migration with the initial model from Figure 19.

To apply the PP + PS = SS method, we registered (correlated) five events on the PP and PS stacked sections. For each of these five events pure shear data were constructed by convolving the computed SS traveltimes with a Ricker wavelet. The codepthing term in the objective function includes the depths of these five reflectors on the PP and SS sections. As expected, the CIGs of PP- and SS-waves obtained with the initial model parameters exhibit substantial residual moveout.

Because of the limited offset-to-depth ratio (smaller than 1.2 for $z > 3$ km), the accuracy of the effective parameters η and ε estimated from nonhyperbolic moveout (i.e., long-spread CIGs) decreases with depth. Therefore, the deeper part of the section ($z > 3$ km) is kept isotropic during model updating. The VTI model obtained after eight iterations of joint MVA of PP- and PS-waves (Figure 21) yields relatively flat PP and SS CIGs and depth-consistent PP and SS images.

The PS-wave depth image generated using PSDM with the estimated VTI model is displayed in Figure 22b. Compared with the section obtained using the initial model (Figure 20b), reflectors on the final image are better focused, especially at depths around 3 km (Cretaceous unit). However, the image quality below the Base Cretaceous unconformity is still lower than that for PP-waves (Figure 22a). This is probably because the deeper layers (below 3 km) are kept isotropic during joint MVA, and PS-waves are more sensitive to anisotropy than PP-waves.

The final PP image (Figure 22a) does not differ much from that obtained by Wang (2012) using P-wave tomography. However, the reflectors in the Cretaceous unit look somewhat less coherent than those imaged by Wang (2012). One possible reason is that Wang (2012) used a larger number of reflectors in building the velocity model. Also, although the dips are gentle, the TTI model employed by Wang (2012) is more geologically plausible and may yield more accurate anisotropy parameters than the VTI model used here. It is likely that better PP and PS depth images can be obtained with a TTI model, but the current version of the algorithm does not allow for a tilt of the symmetry axis.

We were able to tie the PP depth image with the PS depth image down to Base Cretaceous unconformity (the deepest event used to generate SS data). These depth-consistent PP and PS sections provide a robust estimate of the V_{P0}/V_{S0} ratio, which can be used for reservoir characterization.
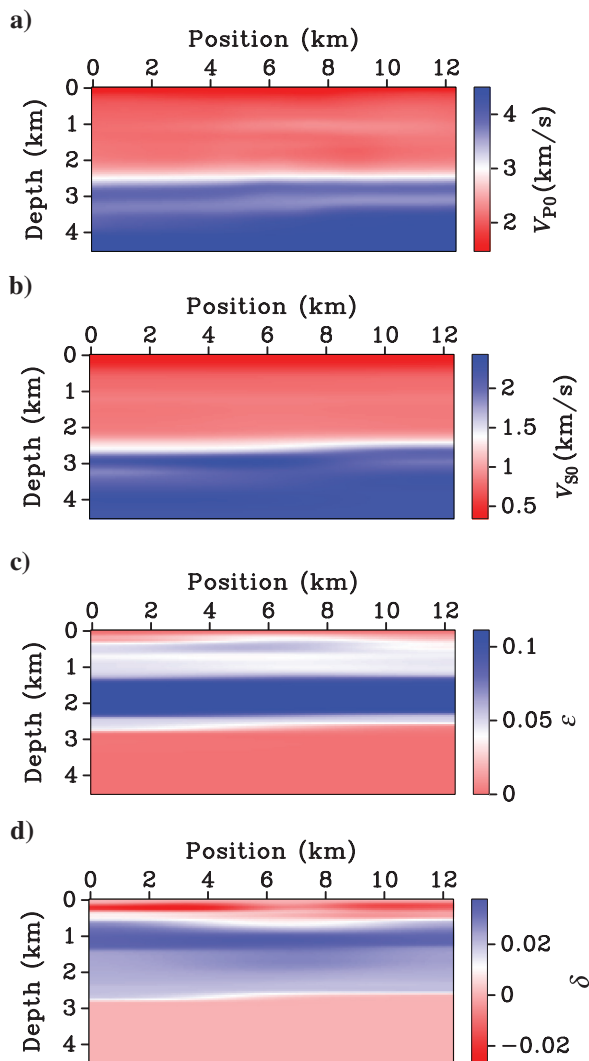

Figure 21. Estimated VTI model for line $y = 2.8$ km from the Volve survey. The vertical velocities (a) V_{P0} and (b) V_{S0} and the anisotropy parameters (c) ε and (d) δ.
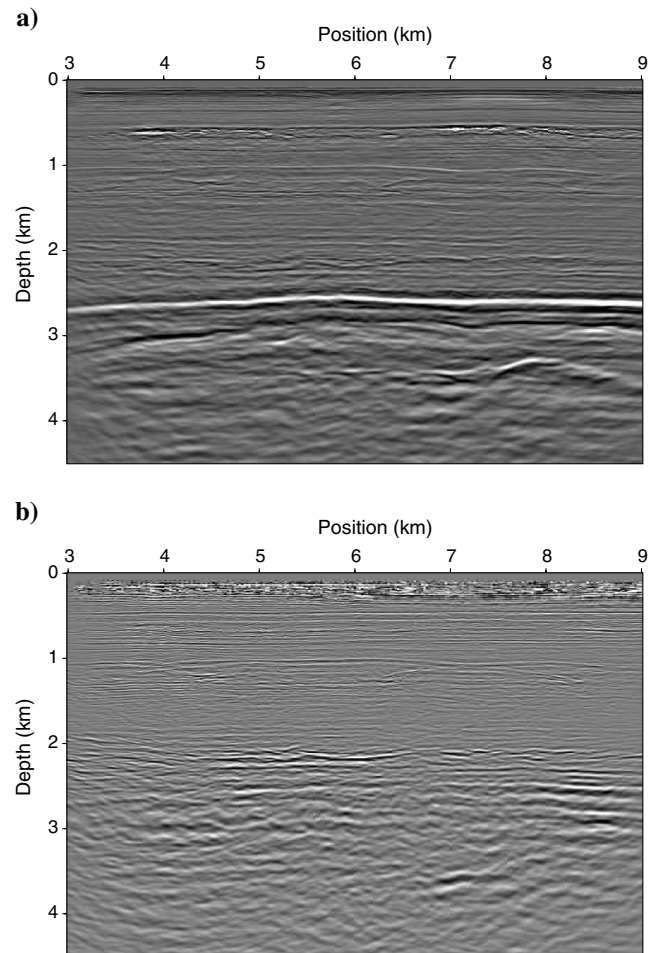

Figure 22. (a) PP- and (b) PS-wave depth images generated with the estimated model from Figure 21.

The final PP- and PS-wave images in Figure 22 are similar to those obtained with the VTI model provided by Statoil. It should be mentioned, however, that Statoil's model has a higher spatial resolution than our model in Figure 21 because our updating procedure operated only with reflection data. Clearly, there is still depth uncertainty in our images, which can be reduced by including borehole (e.g., VSP) information.

CONCLUSIONS

In the presence of moderate dips, combining PP reflection traveltimes with converted PS data may help reconstruct VTI velocity models in depth. Here, we presented an efficient algorithm for joint MVA of PP- and PS-waves from heterogeneous VTI media.

To avoid problems caused by the moveout asymmetry and other undesirable inherent features of mode conversions, we first construct pure SS reflections using the PP + PS = SS method. Implementation of the PP + PS = SS method requires event registration, or identification of PP and PS reflections from the same interfaces. Then MVA is performed for PP and SS data, which allows us to employ existing tomographic techniques devised for pure modes. After performing prestack Kirchhoff depth migration of PP and SS data, we use a nonhyperbolic semblance scan to evaluate the long-spread PP-wave residual moveout in CIGs. Then the velocity model is updated iteratively by simultaneously minimizing the residual moveout in PP- and SS-wave gathers and misties between PP and SS sections.

Synthetic testing for VTI media composed of homogeneous layers confirmed that if both horizontal and moderately dipping PP and PS events are available, the joint MVA of 2D data may converge toward the correct depth model. The inversion becomes generally nonunique in the presence of laterally heterogeneous horizons. However, the parameters of factorized VTI layers can be resolved by correctly assuming that the velocities V_{P0} and V_{S0} vary linearly in space, and ε and δ are constant in each layer. The algorithm produces an acceptable approximation for the velocity field even if V_{P0} and V_{S0} are updated at each grid point, but the resulting image is not as well focused as the one obtained with linear $V_{P0}(x, z)$ and $V_{S0}(x, z)$ functions. Synthetic examples show that velocity estimation on a grid benefits from assigning larger weights to CIG flattening during initial iterations. At later stages of the inversion, however, the convergence is improved by emphasizing the terms of the objective function responsible for codepthing and regularization.

The method was also applied to PP and PS(PSV) data recorded on a 2D line from a 3D OBS survey acquired at Volve field in the North Sea. A VTI model obtained by joint tomography of the recorded PP-waves and constructed SS-waves produced generally well-focused PP and PS depth images. The depth consistency between the PP and PS sections also corroborates the accuracy of the velocity-analysis algorithm.

Our results confirm that PS-waves can play an important role in velocity model building for prestack depth migration. Multicomponent data also provide estimates of the shear-wave vertical velocity V_{S0}, which can be used in lithology prediction and reservoir characterization.

ACKNOWLEDGMENTS

APPENDIX A

PARAMETER-UPDATING METHODOLOGY

We extend the MVA algorithm of Wang and Tsvankin (2013) to the combination of PP and SS data, where the SS-waves are constructed by the PP + PS = SS method. In addition to flattening PP and SS image gathers, we also perform codepthing to ensure that the reflectors on the PP and SS sections are imaged at the same depth. Following Wang and Tsvankin (2013), the variance Var of the migrated depths can be written as

$$\text{Var} = \sum_{j=1}^{U} \sum_{k=1}^{M} [z(x_j, h_k) - \hat{z}(x_j)]^2, \qquad \text{(A-1)}$$

where U is the number of image gathers used in the velocity update, M is the number of offsets in image gathers, x_j is the midpoint, h_k is the half-offset, and $\hat{z}(x_j) = (1/M) \sum_{k=1}^{M} z(x_j, h_k)$ is the average migrated depth at x_j. By minimizing the variances Var_P (for P-waves) and Var_S (for S-waves), we flatten CIGs for both modes. The difference between the migrated depths of PP- and SS-waves from the same reflector can be estimated as

$$\text{Var}_{P-S} = \sum_{j=1}^{U} [\hat{z}_p(x_j) - \hat{z}_s(x_j)]^2. \qquad \text{(A-2)}$$

Minimizing Var_{P-S} makes it possible to tie the PP and SS sections in depth. Differentiating the variances with respect to the parameter updates $\Delta\lambda$ and setting $\partial\text{Var}/\partial(\Delta\lambda) = 0$ yields

$$\mathbf{A}_P^T \mathbf{A}_P \Delta\lambda = -\mathbf{A}_P^T \mathbf{b}_P, \qquad \text{(A-3)}$$

$$\mathbf{A}_S^T \mathbf{A}_S \Delta\lambda = -\mathbf{A}_S^T \mathbf{b}_S, \qquad \text{(A-4)}$$

$$\mathbf{D}^T \mathbf{D}\Delta\lambda = -\mathbf{D}^T \mathbf{y}, \qquad \text{(A-5)}$$

where $\mathbf{A}$ is a $M \times U$ by $W \times N$ matrix with elements $g_{jk,ic} - \hat{g}_{j,ic}$, where $g_{jk,ic} = \partial z(x_j, h_k)/\partial\lambda_{ic}$ and $\hat{g}_{j,ic} = (1/M) \sum_{k=1}^{M} g_{jk,ic}$; the subscripts P and S denote P- and S-waves, respectively. The vector $\mathbf{b}$ contains $M \times U$ elements defined as $z(x_j, h_k) - \hat{z}(x_j)$; $\mathbf{D}$ is also a $M \times U$ by $W \times N$ matrix with elements $g_{jk,ic}^P - g_{jk,ic}^S$, where $g_{jk,ic}^P$ is computed for P-waves and $g_{jk,ic}^S$ for S-waves. The $M \times U$ vector $\mathbf{y}$ has elements $z^P(x_j, h_k) - z^S(x_j, h_k)$. As discussed in Wang and Tsvankin (2013), the derivatives $g_{jk,ic}$ are found by differentiating

phase velocity with respect to the medium parameters along the raypath.

REFERENCES

Adler, F., R. Baina, M. A. Soudani, P. Cardon, and J. Richard, 2008, Nonlinear 3D tomographic least-squares inversion of residual moveout in Kirchhoff prestack-depth-migration common-image gathers: Geophysics, **73**, no. 5, VE13–VE23, doi: 10.1190/1.2956427.

Audebert, F., P. Y. Granger, and A. Herrenschmidt, 1999, CCP-scan technique (1): True common conversion point sorting and converted wave velocity analysis solved by PP and PS pre-stack depth migration: 69th Annual International Meeting, SEG, Expanded Abstracts, 1186–1189.

Bakulin, A., M. Woodward, D. Nichols, K. Osypov, and O. Zdraveva, 2010, Building tilted transversely isotropic depth models using localized anisotropic tomography with well information: Geophysics, **75**, no. 4, D27–D36, doi: 10.1190/1.3453416.

Broto, K., A. Ehinger, J. H. Kommedal, and P. G. Folstad, 2003, Anisotropic traveltime tomography for depth consistent imaging of residual PP and PS data: The Leading Edge, **22**, 114–119, doi: 10.1190/1.1559037.

Du, Q., F. Li, J. Ba, Y. Zhu, and B. Hou, 2012, Multicomponent joint migration velocity analysis in the angle domain for PP-waves and PS-waves: Geophysics, **77**, no. 1, U1–U13, doi: 10.1190/geo2010-0423.1.

Foss, S.-K., B. Ursin, and M. V. de Hoop, 2005, Depth-consistent reflection tomography using PP and PS seismic data: Geophysics, **70**, no. 5, U51–U65, doi: 10.1190/1.2049350.

Gajewski, D., and I. Pšenčík, 1987, Computation of high-frequency seismic wavefields in 3-D laterally inhomogeneous anisotropic media: Geophysical Journal of the Royal Astronomical Society, **91**, 383–411, doi: 10.1111/j.1365-246X.1987.tb05234.x.

Grechka, V., and P. Dewangan, 2003, Generation and processing of pseudo-shear-wave data: Theory and case study: Geophysics, **68**, 1807–1816, doi: 10.1190/1.1635033.

Grechka, V., A. Pech, and I. Tsvankin, 2002a, Multicomponent stacking-velocity tomography for transversely isotropic media: Geophysics, **67**, 1564–1574, doi: 10.1190/1.1512802.

Grechka, V., and I. Tsvankin, 2002a, The joint nonhyperbolic moveout inversion of PP and PS data in VTI media: Geophysics, **67**, 1929–1932, doi: 10.1190/1.1527093.

Grechka, V., and I. Tsvankin, 2002b, PP + PS = SS: Geophysics, **67**, 1961–1971, doi: 10.1190/1.1527096.

Grechka, V., I. Tsvankin, A. Bakulin, J. O. Hansen, and C. Signer, 2002b, Joint inversion of PP and PS reflection data for VTI media: A North Sea case study: Geophysics, **67**, 1382–1395, doi: 10.1190/1.1512784.

Sarkar, D., and I. Tsvankin, 2004, Migration velocity analysis in factorized VTI media: Geophysics, **69**, 708–718, doi: 10.1190/1.1759457.

Stopin, A., and A. Ehinger, 2001, Joint PP/PS tomographic inversion of the Mahogany 2D 4-C OBC seismic data: 71st Annual International Meeting, SEG, Expanded Abstracts, 837–840.

Stork, C., 1992, Reflection tomography in the postmigrated domain: Geophysics, **57**, 680–692, doi: 10.1190/1.1443282.

Szydlik, T., P. Smith, S. Way, L. Aamodt, and C. Friedrich, 2007, 3D PP/PS prestack depth migration on the Volve field: First Break, **25**, 43–47.

Thomsen, L., 1999, Converted-wave reflection seismology over inhomogeneous, anisotropic media: Geophysics, **64**, 678–690, doi: 10.1190/1.1444577.

Tsvankin, I., 2005, Seismic signatures and analysis of reflection data in anisotropic media, 2nd ed.: Elsevier Science Publishing Company, Inc.

Tsvankin, I., and V. Grechka, 2000, Dip moveout of converted waves and parameter estimation in transversely isotropic media: Geophysical Prospecting, **48**, 257–292, doi: 10.1046/j.1365-2478.2000.00181.x.

Tsvankin, I., and V. Grechka, 2011, Seismology of azimuthally anisotropic media and seismic fracture characterization: SEG.

Tsvankin, I., and L. Thomsen, 1995, Inversion of reflection traveltimes for transverse isotropy: Geophysics, **60**, 1095–1107, doi: 10.1190/1.1443838.

Wang, B., K. Pann, and R. A. Meek, 1995, Macro velocity model estimation through model based globally-optimized residual-curvature analysis: 65th Annual International Meeting, SEG, Expanded Abstracts, 1084–1087.

Wang, X., 2012, Anisotropic velocity analysis of P-wave reflection and borehole data: Ph.D. thesis, Colorado School of Mines.

Wang, X., and I. Tsvankin, 2010, Stacking-velocity inversion with borehole constraints for tilted TI media: Geophysics, **75**, no. 5, D69–D77, doi: 10.1190/1.3481652.

Wang, X., and I. Tsvankin, 2013, Ray-based gridded tomography for tilted transversely isotropic media: Geophysics, **78**, no. 1, C11–C23, doi: 10.1190/geo2012-0066.1.

Zhou, C., J. Jiao, S. Lin, J. Sherwood, and S. Brandsberg-Dahl, 2011, Multiparameter joint tomography for TTI model building: Geophysics, **76**, no. 5, WB183–WB190, doi: 10.1190/geo2010-0395.1.